J Mater Sci (2006) 41:4737–4743
DOI 10.1007/s10853-006-0044-5

# Preparation of manganese molybdate rods and hollow olive-like spheres

**Shuijin Lei · Kaibin Tang · Qiangchun Liu · Zhen Fang · Qing Yang · Huagui Zheng**

Received: 13 June 2005 / Accepted: 19 September 2005 / Published online: 4 May 2006


**Abstract** Stable phase alpha-manganese molybdate ($\alpha$-$MnMoO_4$) rods, wolframite structure $MnMoO_4$ hollow olive-like spheres and hexahedron-like manganese molybdate monohydrate ($MnMoO_4 \cdot H_2O$) were selectively synthesized by a simple hydrothermal method at 150–200 °C. Experiments showed that the reaction temperature, pH, molybdenum source and ligand played very important roles in controlling the polymorph and morphologies of the product. The samples were characterized by X-ray powder diffraction and scanning electron microscopy. Possible formation process of the product was proposed.

## Introduction

Recently, the divalent transition-metal group six metal oxides ($MXO_4$, X = Cr, Mo, W) have attracted intensive interest due to their novel chemical and physical properties (for example magnetic) and potential wide-ranging applications. $BaCrO_4$ chains and filaments, $BaCrO_4$ and $BaWO_4$ nanorods or nanowires have been successfully synthesized in reverse micelles and microemulsion techniques [1–6]. Yu et al. have prepared highly ordered funnel-like $BaCrO_4$ by polymer-controlled mineralization reactions [7]. A solvothermal route was used to prepare $MnWO_4$ nanoparticles and nanorods by Chen et al. [8]. Clearfield et al. [9, 10] have reported the preparation of zinc molybdate from aqueous solution and resolved its structure.

Manganese molybdate exhibits interesting magnetic, catalytic, electrochemical properties and spectral features [11–18]. $MnMoO_4$ has three polymorphs: $\alpha$-$MnMoO_4$ is usually prepared by high-temperature solid-state reactions and is the polymorph stable under ambient conditions of temperature and pressure [11, 19–21]. Another phase of $MnMoO_4$, with wolframite structure (W-$MnMoO_4$), is obtained from the reaction of MnO with $MoO_3$ at high pressure (60 kbar) and high temperature (900 °C), which can convert to $\alpha$-$MnMoO_4$ if heated in air at 60 °C for 2 days [22]. The third phase of $MnMoO_4$ is isostructural with $CoMnO_4$ [21]. The structure of $\alpha$-$MnMoO_4$ is composed of octahedrally coordinated Mn atoms and tetrahedrally coordinated Mo atoms by oxygen atoms with space group C2/m [21, 23]. Whereas, for W-$MnMoO_4$, with space group P2/c, each Mn and Mo atom is in an approximately octahedral coordination surrounded by six near oxygen atom sites [24, 25], viz. oxygen atoms forming a distorted hexagonal close packing with each Mn and Mo atom occupying one-fourth of the octahedral interstitial sites [22]. In the third structure of $MnMoO_4$, different from $\alpha$-$MnMoO_4$, in which Mo atom has a somewhat distorted tetrahedral coordination, Mo atom is in a highly distorted octahedral coordination [21].

Traditionally, crystalline $MnMoO_4$ was synthesized using a solid stable reaction of $MoO_3$ with manganese oxides or by precipitation from aqueous solutions of soluble salts at high temperature or/and high pressure [26, 27]. A lower valent molybdate of the type $Mn_2Mo_3O_8$ was also

S. Lei · K. Tang (✉) · Q. Liu · Z. Fang · Q. Yang
Nanomaterial and Nanochemistry, Hefei National Laboratory for Physical Sciences at Micro-scale, University of Science and Technology of China, Hefei, Anhui 230026, P.R. China
e-mail: kbtang@ustc.edu.cn

H. Zheng
Department of Chemistry, University of Science and Technology of China, Hefei, Anhui 230026, P.R. China

prepared by reduction at high temperatures [28]. A variety of hydrated manganese (II) molybdenum oxides have also been prepared by aqueous metathesis reactions [9, 23, 29]. For example, Corbet et al. [26] have reported the synthesis of $MnMoO_4{\cdot}0.9H_2O$ and Sinhamahapatra et al. [30] have obtained $MnMoO_4{\cdot}1.5H_2O$ by precipitation from ammonium molybdate and manganese sulfate solutions at 80–90 °C.

Herein, a simple hydrothermal method was used to prepare α-$MnMoO_4$ rods, wolframite structural $MnMoO_4$ hollow olive-like spheres and $MnMoO_4{\cdot}H_2O$ hexahedrons. The effects of the reaction temperature, pH, molybdenum source, and ligand on the polymorph and the morphology of the product were investigated.

## Experimental

### Preparation of α-$MnMoO_4$ rods

All the chemical reagents are analytically pure and purchased from Shanghai Chemical Reagent Company and used as received without further purification. In a typical procedure, $MoO_3$ (0.288 g, 2 mmol), a slight excess of solid NaOH (0.17 g, 4.25 mmol) and about 20 mL distilled water were put into a Teflon-lined autoclave of 60 mL capacity and stirred to be a clear solution. A volume of 0.05 M tartaric acid (TA) solution was added dropwise to adjust the pH of the system to be around 6–7, and $MnCl_2{\cdot}4H_2O$ (0.396 g, 2mmol) was added into the solution in succession with stirring to deposit homogeneously. The autoclave was filled with distilled water up to 90% of the total volume, sealed and maintained at 200 °C for 12 h and then cooled to room temperature naturally. The precipitate was filtered off and washed with absolute ethanol and distilled water several times to remove impurities. After being dried in vacuum at 60 °C for 4 h, the final beige product was collected for characterization.

### Preparation of W-$MnMoO_4$ hollow olive-like spheres

Upon replacement of $MoO_3$ with ammonium molybdate monohydrate $(NH_4)_6Mo_7O_{24}{\cdot}H_2O$) and a decrease of the reaction temperature to 180 °C, with other conditions identical, then a black powder was obtained.

### Preparation of $MnMoO_4{\cdot}H_2O$ hexahedrons

In both procedures above, if the reaction temperature was decreased to 150 °C keeping other conditions constant, then the product obtained was gray.

The detailed contrast experiments were outlined in Table 1.

### Characterizations of various samples

The X-ray powder diffraction (XRD) patterns were collected on a Philips X′pert PRO SUPER diffractometer with Cu-Kα radiation ($\lambda$ = 1.54187 Å). The scanning electron microscopy (SEM) images were taken with an X-650 scanning electronic microanalyzer. Infrared (IR) spectra were characterized on a Bruker Vector-22 IR spectrometer from 4000 $cm^{-1}$ to 400 $cm^{-1}$ at room temperature. The samples were dispersed in KBr (1.5/150 mg) and pressed in transparent disks, which were employed for the measurement of IR spectra. Meanwhile, electron spin resonance (ESR) spectra were recorded on a Bruker model ER-200D SRC-10/12 instrument with the magnetic field ranged from 0 to 800 mT, microwave frequency 9064.414 MHz and the modulation frequency 100 kHz at room temperature.

**Table 1** Outline of the experiments and the influence of the reaction temperature, pH, Mo source and acid on the polymorph and the morphologies of the product

| Sample | Reaction temperature (°C) | pH | Mo source | Ligand | Product | Morphology |
|---|---|---|---|---|---|---|
| S1 | 200 | 6–7 | $MoO_3$ | TA | α-$MnMoO_4$ | Rods |
| S2 | 200 | 6–7 | $(NH_4)_6Mo_7O_{24}{\cdot}H_2O$ | TA | α-$MnMoO_4$ | Rods & Flakes |
| S3 | 180 | 7–8 | $MoO_3$ | TA | α-$MnMoO_4$ | Rods |
| S4 | 180 | 7–8 | $(NH_4)_6Mo_7O_{24}{\cdot}H_2O$ | TA | α-$MnMoO_4$ | Rods |
| S5 | 180 | 6–7 | $(NH_4)_6Mo_7O_{24}{\cdot}H_2O$ | CA | α-$MnMoO_4$ | Rods |
| S6 | 180 | 6–7 | $(NH_4)_6Mo_7O_{24}{\cdot}H_2O$ | HCl | α-$MnMoO_4$ | Rods |
| S7 | 180 | 6–7 | $(NH_4)_6Mo_7O_{24}{\cdot}H_2O$ | TA | W-$MnMoO_4$ | Hollow olive-like spheres |
| S8 | 180 | 10–11 | $MoO_3$ | / | W-$MnMoO_4$ | Irregular crystals |
| S9 | 150 | 6–7 | $MoO_3$ | TA | $MnMoO_4{\cdot}H_2O$ | Irregular hexahedrons |
| S10 | 150 | 6–7 | $(NH_4)_6Mo_7O_{24}{\cdot}H_2O$ | TA | $MnMoO_4{\cdot}H_2O$ | Irregular hexahedrons |
| S11 | 180 | 6–7 | $MoO_3$ | TA | $MnMoO_4{\cdot}H_2O$ | Hexahedrons & Flakes |
| S12 | 180 | 10–11 | $(NH_4)_6Mo_7O_{24}{\cdot}H_2O$ | / | $MnMoO_4{\cdot}H_2O$ | Flakes |

Notes: TA stands for tartaric acid and CA for citric acid

## Results and discussion

### XRD analysis

Figure 1 shows the XRD patterns of some as-synthesized samples (S1, S2, S6 in Table 1). In Fig. 1a, all the diffraction peaks can be indexed as the monoclinic α-$MnMoO_4$ with lattice parameters $a = 10.501 \pm 0.022$ Å, $b = 9.541 \pm 0.012$ Å, $c = 7.170 \pm 0.011$ Å, and $\beta = 106.254 \pm 0.082°$, which are consistent with reported values (Joint Committee on Powder Diffraction Standards (JCPDS), Powder Diffraction File No. 72-0285, $a = 10.46$ Å, $b = 9.516$ Å, $c = 7.143$ Å and $\beta = 106.28°$). From Fig. 1a, it is found that the diffraction peaks due to hh0 and $\bar{h}$hh index are stronger than those reported in the JCPDS card, which indicates a growth orientation of the (110) and ($\bar{1}$11) planes in the as-prepared crystals.

The XRD patterns of the samples (S7 and S8) are shown in Fig. 2, which can be indexed to the wolframite structure $MnMoO_4$ with $a = 4.825 \pm 0.002$ Å, $b = 5.773 \pm 0.002$ Å, $c = 4.978 \pm 0.002$ Å, and $\beta = 90.861 \pm 0.022°$, corresponding to reported data (JCPDS File No. 78-0221, $a = 4.818$ Å, $b = 5.759$ Å, $c = 4.965$ Å, and $\beta = 90.82°$). Compared to the JCPDS card, there also exist evident changes of the relative intensity of the diffraction peaks. In Fig. 2b, the relative intensities of 010, 100, 011 diffraction peaks become stronger, and the 100 peak turns to be the strongest one, which also reveals the growth orientation in the crystals.

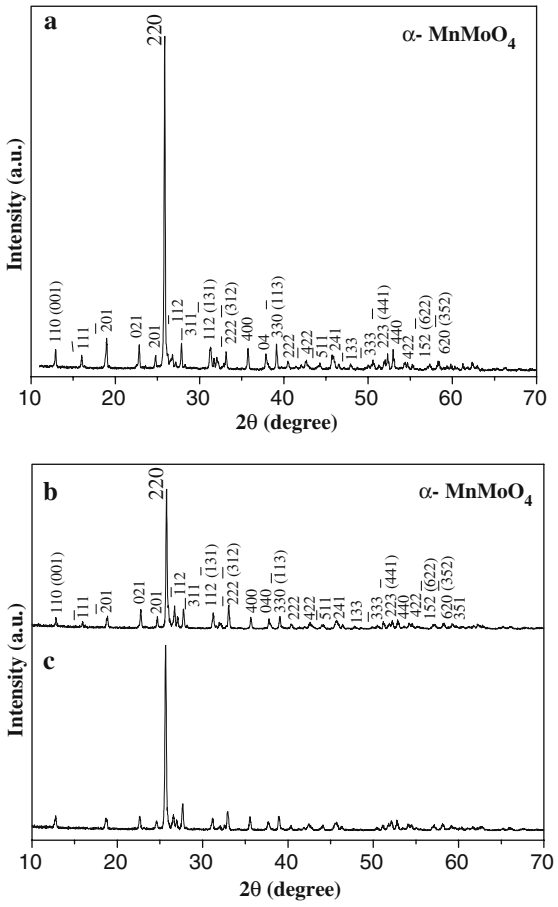


**Fig. 1** XRD patterns of some as-prepared samples for: (**a**) S1, (**b**) S2, and (**c**) S6

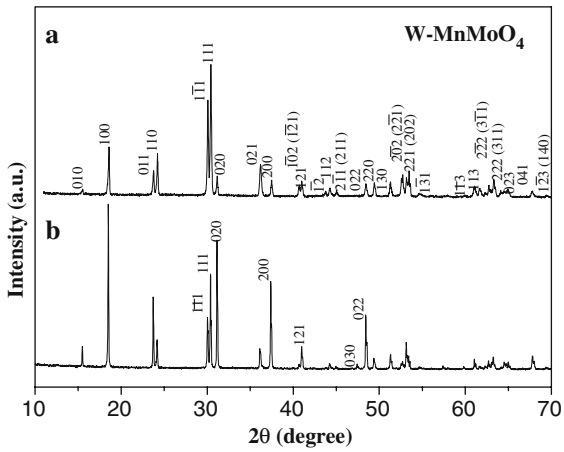


**Fig. 2** XRD patterns of the samples for: (**a**) S7, and (**b**) S8

Figure 3 gives the XRD patterns of some other samples (S9, S10 and S12). All peaks agree with the reflections of anorthic $MnMoO_4 \cdot H_2O$ with $a = 5.799 \pm 0.008$ Å, $b = 5.986 \pm 0.009$ Å, $c = 7.018 \pm 0.009$ Å and $\alpha = 100.141 \pm 0.101°$, $\beta = 95.689 \pm 0.126°$, $\gamma = 106.829 \pm 0.079°$, consistent with reported data (JCPDS, Powder Diffraction File No.78-0220, $a = 5.776$ Å, $b = 5.964$ Å, $c = 6.992$ Å, and $\alpha = 100.32°$, $\beta = 95.56°$, $\gamma = 106.81°$). In this figure, there is an obvious contrast of the intensity of the diffraction peaks. For Fig. 3c, the relative intensity of $\bar{1}$10, and 110 (002) diffraction peaks becomes stronger. Especially in Fig. 3a, the $\bar{1}$10 diffraction peak is extremely strong. All those imply a preferential growth in products.

### SEM analysis

The morphologies of the products were observed by SEM. Figure 4a and b reveal the SEM images of as-prepared α-$MnMoO_4$ (S1), which shows that the product is composed of a large amount of rods 5–20 μm in length and 1–2 μm in width of the section. XRD pattern (Fig. 1a) has shown the growth orientation of (110) and ($\bar{1}$11) plane, the interplanar angle of (110) and ($\bar{1}$11) plane is calculated to be 80.8°. Hence, the lengthways sides of the rods are expected to be (110) and ($\bar{1}$11) planes, and the rods were grown along [0$\bar{1}$1] zone axis of (110) and ($\bar{1}$11) planes. Figure 4c and d (for S5 and S6) also shows rods, but they are shorter and less regular than those in Fig. 4a and b. And Fig. 4e presents flake morphology for α-$MnMoO_4$ (S2).

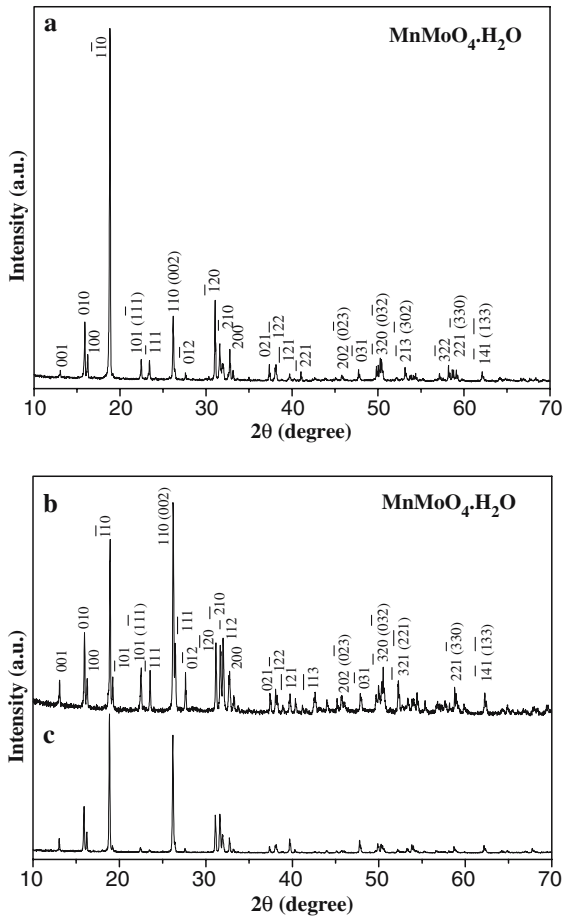


**Fig. 3** XRD patterns of the samples for: (**a**) S12, (**b**) S10, and (**c**) S11

The W-$MnMoO_4$ hollow olive-like spheres are shown in Fig. 5a–d (for S7). The direct observation of the broken olive-like sphere affords the strongest evidence for their hollow nature, as shown in Fig. 5d and marked-frames. Due to the spherical morphology, no evident tropism can be detected in the corresponding XRD patterns (Fig. 2a). The irregular crystals of W-$MnMoO_4$ are shown in Fig. 5e (for S8), in which some quasi-hexagonal crystals can be observed. From the XRD patterns in Fig. 2b, the growth orientation planes of crystal should be (100), (011), (010) etc. The interplanar angles between (100) and (011), (010), $(01\bar{1})$ plane are calculated as 90°, 89.4°, and 90.6°, respectively. The interplanar angles between (010) and (011), $(01\bar{1})$ plane are both 49.2°, and the interplanar angle of $(01\bar{1})$ and $(0\bar{1}\bar{1})$ is 81.5°. Therefore, the planes of quasi-hexagonal crystals are expected to be (100), (011), (010) and $(01\bar{1})$ (Fig. 5e).

Figure 6a–c presents $MnMoO_4{\cdot}H_2O$ irregular hexahedrons and flakes images. The flakes shown in Fig. 6b were grown along $(\bar{1}10)$ plane orientation, which results in the strong $\bar{1}10$ diffraction peak in the XRD patterns (Fig. 3a). The interplanar angles between $(\bar{1}10)$ and (110), (002) plane are 91.2° and 87.3°, and the interplanar angle of (110) and (002) plane is 76.7°. Those all can be observed in the image (Fig. 6a) and reflected on the relative tropisms in the XRD patterns (Fig. 3c).

Normally, $MnMoO_4$ crystallites prepared from the direct precipitation were often relatively large and exhibited varied grain size and irregular morphology. $MnMoO_4$ rods may be useful to the electrochemical and optical properties as a result of their low dimensionality [31], while $MnMoO_4$ three-dimensional (3D) hollow olive-like spheres should be useful to improve the catalytic property due to the large specific surface area of their hollow structure [32]. It is reasonable to think that the oriented growth of $MnMoO_4$ rods and flakes should be important for the spectral property.

## IR and ESR analysis

Figure 7a and b show the IR spectra of as-synthesized α-$MnMoO_4$ and W-$MnMoO_4$. In both spectra, the absorption bands observed at 3434–3437 $cm^{-1}$ and 1619–1639 $cm^{-1}$ are attributable to OH vibrations due to water contamination on the surface. In Fig. 7a, there are four bands in a very similar position ($\gamma$ ($cm^{-1}$)): 943, 861, 796, 715. These analogies confirm that α-$MnMoO_4$ has a tetrahedral coordination of Mo at the surface. Band at 943 $cm^{-1}$ is typically attributed to the Mo=O groups [33]. It is found that a number of intense absorption bands in the range of 700–943 $cm^{-1}$ can be observed, two of which are characteristic of tetrahedral $MoO_4$ groups, while three more should result from octahedral $MnO_6$ groups [23, 34].

Figure 8a and b show the ESR spectra of as-synthesized α-$MnMoO_4$ and W-$MnMoO_4$. It can be seen that the center of the magnetic field in both curves is located at almost the same position. The difference is that line 8a is clearly narrower than line 8b. These resonance curves correspond to a typical signal of paramagnetic $Mn^{2+}$ ion with a poorly resolved hyperfine structure, and further affirm the existence of Mn coordination in the ionic lattice. The observed ESR signals were symptomized by their $g$ factor (Lande factor), which is defined by $g = h\gamma/\beta H$, where $g$ is a parameter describing the interaction of the paramagnetic center with the external magnetic field, $h$ is the Planck's constant, $\gamma$ is the microwave frequency, $\beta$ is the Bohr magneton and $H$ is the intensity of the resonance magnetic field. Calculated from the formula above, $g = 1.619$ can be obtained.

## Discussions of the effects of the reaction conditions

In the reaction process, there are four major factors influencing the polymorph and morphologies, viz. the pH, reaction temperature, molybdenum source, and ligand. Table 1 gives the summary of the experiments and results,

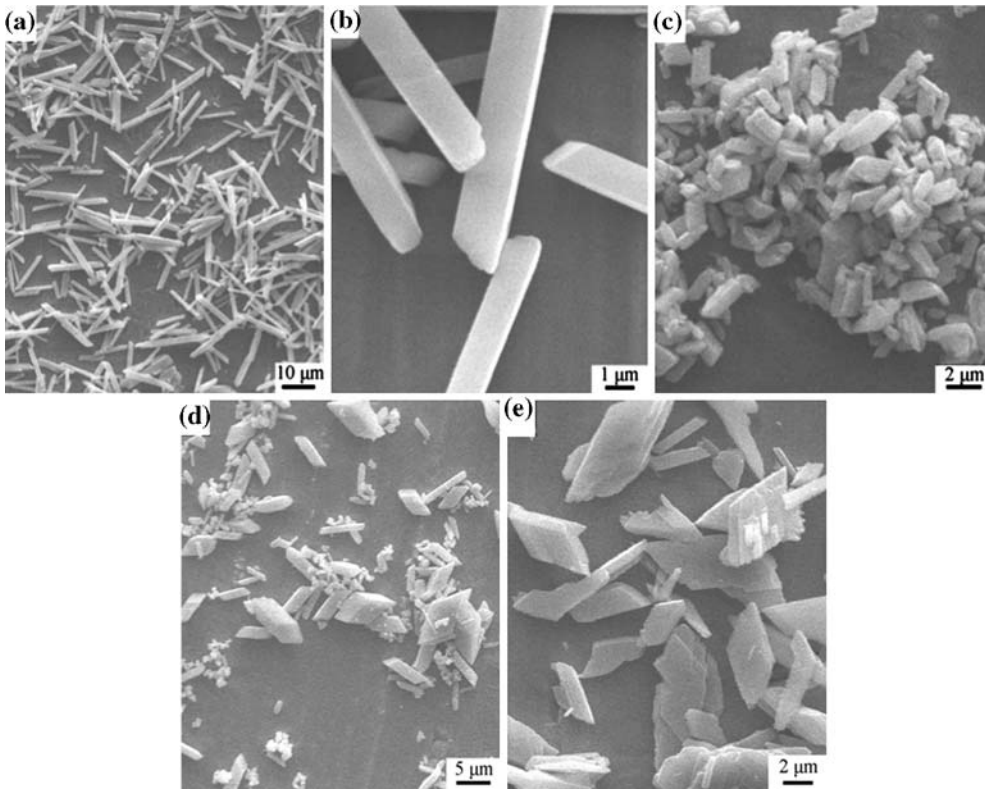


**Fig. 4** SEM images of as-prepared α-$MnMoO_4$: (**a**, **b**) S1, (**c**) S5, (**d**) S6 and (**e**) S2

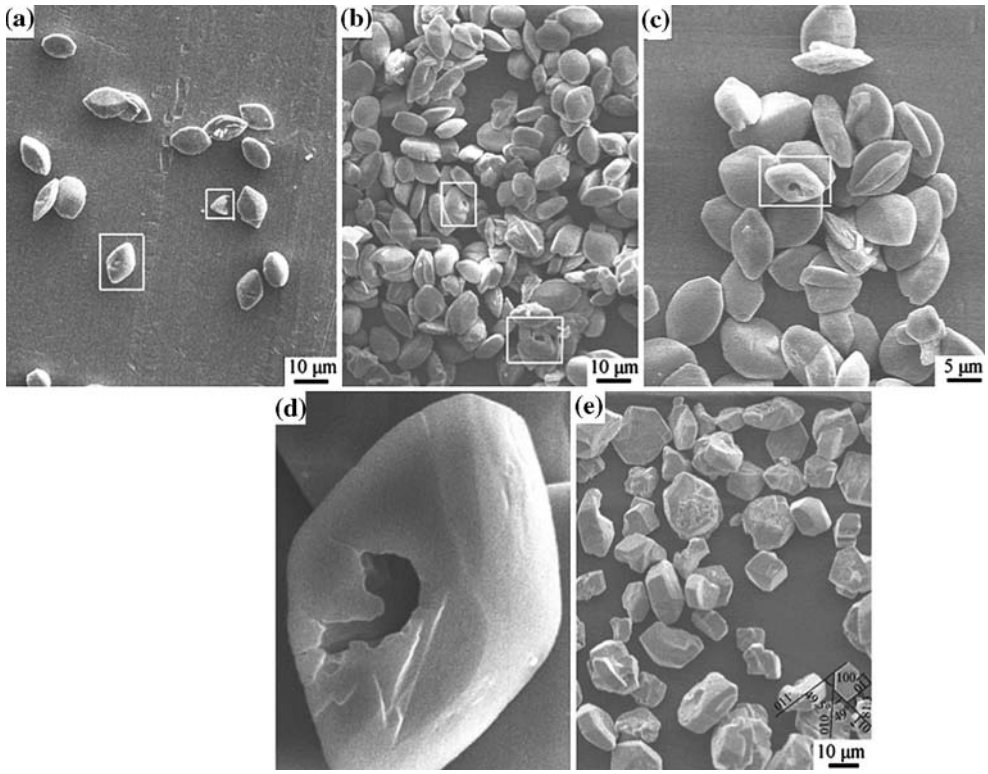


**Fig. 5** SEM images of as-prepared W-$MnMoO_4$: (**a**–**c**) S7, (**d**) a broken hollow quasi-sphere magnified from marked-frame in (**c**) and (**e**) S8

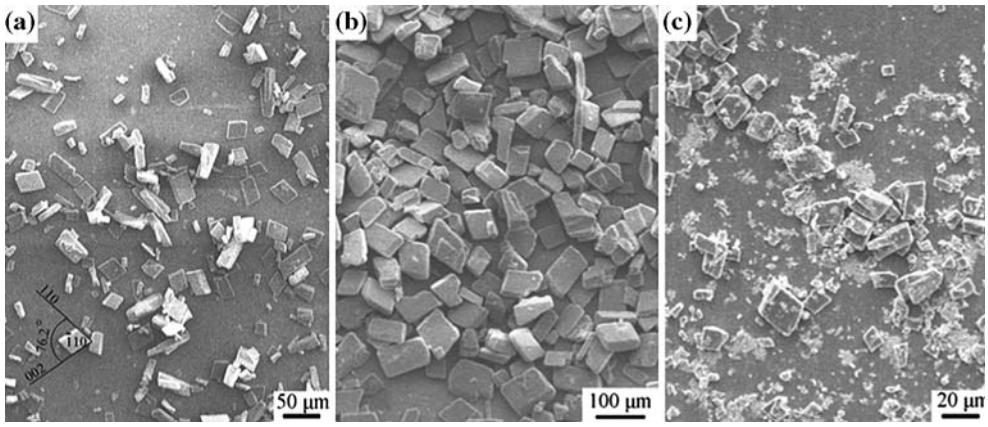


**Fig. 6** SEM images of as-prepared $MnMoO_4 \cdot H_2O$: (**a**) S11, (**b**) S12 and (**c**) S10

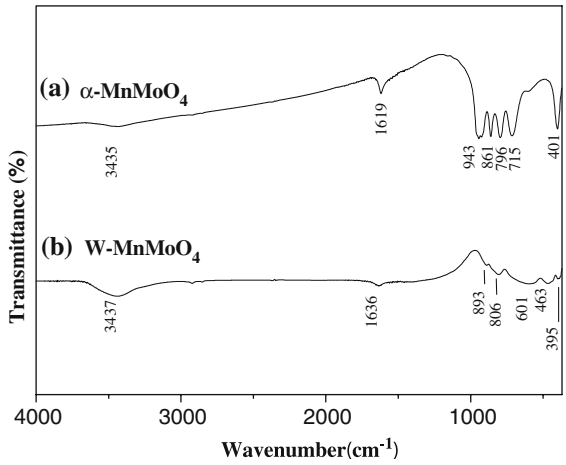


**Fig. 7** IR spectra of the samples: (**a**) $\alpha$-$MnMoO_4$ and (**b**) W-$MnMoO_4$

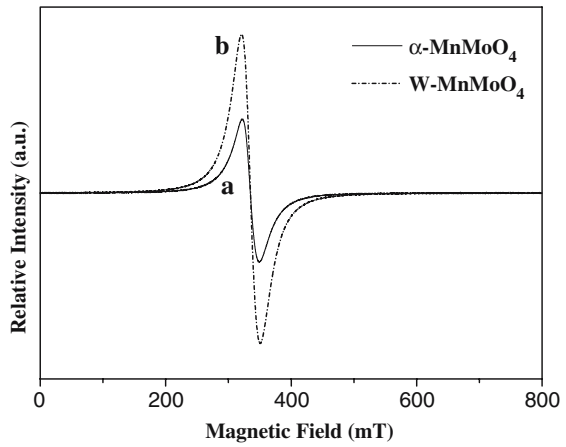


**Fig. 8** ESR spectra of the samples: (**a**) $\alpha$-$MnMoO_4$ and (**b**) W-$MnMoO_4$

from which the influence of the pH, reaction temperature, molybdenum source, and ligand on the polymorph and the morphologies of the product can be clearly deduced.

The reaction temperature affects the polymorph of the product greatly. Keeping the pH (6–7), molybdenum source ($(NH_4)_6Mo_7O_{24} \cdot H_2O$), and ligand (TA) identical, $\alpha$-$MnMoO_4$, W-$MnMoO_4$, and $MnMoO_4 \cdot H_2O$ were obtained at 200, 180, and 150 °C, respectively (S2, S7 and S10). It indicates that the higher reaction temperature is favorable for the formation of the most stable phase $\alpha$-$MnMoO_4$.

The effects of the pH and molybdenum source on the polymorph of the product were also investigated. When $MoO_3$ was used as molybdenum source, if the pH was 6–7, $MnMoO_4 \cdot H_2O$ was prepared at 180 °C (S11). But if pH = 7–8 and 10–11, then $\alpha$-$MnMoO_4$ and W-$MnMoO_4$ were produced, respectively (S3 and S8). Replacement of $MoO_3$ with $(NH_4)_6Mo_7O_{24} \cdot H_2O$, the product was W-$MnMoO_4$, $\alpha$-$MnMoO_4$, and $MnMoO_4 \cdot H_2O$ if the pH was controlled at 6–7, 7–8, and 10–11, respectively (S7, S4 and S12). The results imply that the neutral or very weak alkaline medium is fit for the formation of $\alpha$-$MnMoO_4$.

The pH, molybdenum source, reaction temperature, and ligand are crucial to the morphology of the products. $\alpha$-$MnMoO_4$ rods were prepared at 200 °C when $MoO_3$ was used as molybdenum source and TA was used to adjust the pH to 6–7 (S1, Fig. 4a, b). If $MoO_3$ was replaced by $(NH_4)_6Mo_7O_{24} \cdot H_2O$, then some flakes appeared (S2, Fig. 4e). While for both molybdenum sources, if the pH was changed to 8–9 from 6–7 and the reaction temperature was decreased to 180 °C, the rods evidently became shorter (S3–S4). Keeping temperature (180 °C) and molybdenum source ($(NH_4)_6Mo_7O_{24} \cdot H_2O$) constant and returning the pH to 6–7, if 0.05 M citric acid (CA) or diluted hydrochloric acid (HCl) was used to adjust the pH instead of TA, then grayish-green and orange red $\alpha$-$MnMoO_4$ powder was yielded (S5 and S6), which maybe results from the coordination of the CA radical and $Cl^-$ with $Mn^{2+}$. And the $\alpha$-$MnMoO_4$ rods also became shorter (Fig. 4c, d).

The influence of the pH and molybdenum source on the morphologies of W-$MnMoO_4$ is very obvious, too. The W-$MnMoO_4$ hollow olive-like spheres were prepared at 180 °C with $(NH_4)_6Mo_7O_{24} \cdot H_2O$ as the molybdenum

source and TA being used to adjust the pH to 6–7 (S7, Fig. 5a–d). When substituting $MoO_3$ for $(NH_4)_6Mo_7O_{24}\cdot H_2O$ and controlling the pH at 10–11 simultaneously, W-$MnMoO_4$ irregular crystals were obtained (S8, Fig. 5e).

For both molybdenum sources, the $MnMoO_4\cdot H_2O$ hexahedrons could be prepared at 150 °C when TA was used to control the pH at 6–7 (S9–S10, Fig. 6c). With $MoO_3$ as the molybdenum source, when the reaction temperature was increased to 180 °C, then some $MnMoO_4\cdot H_2O$ flakes were formed (S11, Fig. 6a). While with $(NH_4)_6Mo_7O_{24}\cdot H_2O$ as the molybdenum source, if the pH was adjusted to 10–11, then only $MnMoO_4\cdot H_2O$ flakes were obtained (S12, Fig. 6b).

### Discussions of formation mechanism

As to the formation mechanism, there is presumably a coordination process. From the above experiments, the color of the filtrate was different evidently when various acids were used to control the pH. If TA was dripped, the filtrate was blue sometimes, while CA and HCl resulted in green and red filtrate, respectively. Mn (II) has a $3d^5$ high spin electron distribution without crystal field stabilization energy, which often forms the 6-coordinate octahedral and 4-coordinate tetrahedral complexes. The large ionic radius of $Mn^{2+}$ results in its small stability constant. Therefore, this common process can be reasonably elucidated as the following three stages: (i) the formation of $MnMoO_4$ by the reaction of $MoO_3$ or $(NH_4)_6Mo_7O_{24}$ with NaOH; (ii) the coordination of $Mn^{2+}$ with TA (or CA, HCl) to form $Mn_{n+1}(C_4O_6H_4)_nMoO_4$ (or $Mn_{n+1}(C_6O_7H_7)_{2n}MoO_4$, $Mn_2Cl_4MoO_4$) complex; and (iii) the decomposition of the complex with the increase of the temperature in the hydrothermal process. The complexes are formed before the hydrothermal process, which can be regarded as the intermediate product.

## Conclusions

In summary, α-$MnMoO_4$ micron-sized rods with uniform dimension and W-$MnMoO_4$ hollow olive-like spheres have been successfully fabricated in high yield via a hydrothermal route at low temperature (180–200 °C). Meanwhile, $MnMoO_4\cdot H_2O$ hexahedrons were also prepared at the relatively lower temperature. It is found that the pH, reaction temperature, molybdenum source, and acid had crucial effects on determining the polymorph and morphologies of the final product. A possible formation mechanism for various polymorphs of the samples was also tentatively proposed and a detailed exploration of the mechanism is needed. It is expected that such a simple hydrothermal method could be extended to prepare other important divalent transition-metal molybdate, even divalent transition-metal group six metal oxides.

**Acknowledgements** Financial supports by the National Natural Science Foundation of China, the 973 Projects of China and the Program for new Century Excellent Talents in university (NCET) are gratefully acknowledged.

## References

1. Pileni MP, Ninham BW, Gulik-Krzywicki T, Tanori J, Lisiecki I, Filankembo A (1999) Adv Mater 11:1358
2. Li M, Schnablegger H, Mann S (1999) Nature 402:393
3. Kim F, Kwan S, Amana J, Yang P (2001) J Am Chem Soc 123:4360
4. Kwan S, Kim F, Akana J, Yang P (2001) Chem Commun 5:447
5. Shi HT, Qi LM, Ma JM, Cheng HM (2002) Chem Commun 16:1704
6. Estroff LA, Hamilton AD (2001) Chem Mater 13:3227
7. Yu SH, Antonietti M, Cölfen H, Hartmann J (2003) Nano Lett 3:379
8. Chen SJ, Chen XT, Xue ZL, Zhou JH, Li J, Hong JM, You XZ (2003) J Mater Chem 13:1132
9. Clearfield A, Sims MJ, Gopal R (1976) Inorg Chem 15:335
10. Clearfield A, Gopal R, Saldarriaga-Molina CH (1977) Inorg Chem 16:628
11. Doyle WP, McGuire G, Clark GM (1966) J Inorg Nucl Chem 28:1185
12. Rajaram P, Viswanathan B, Sastri MVC, Srinivasan V (1974) Indian J Chem 12:1267
13. Veleva S, Trifiro F (1976) Kinet Catal Lett 4:19
14. Uitert LGV, Sherwood RC, Williams HJ, Rubin JJ, Bonner WA (1964) J Phys Chem Solids 25:1447
15. Attfield JP (1990) J Phys Condens Matter 2:6999
16. Lippold B, Herrmann J, Reichelt W, Oppermann H (1991) Phys Status Solidi A124:K59
17. Lautenschlager G, Weitzel H, Fuess H, Ressouche EZ (1994) Kristallografiya 209:936
18. Sung-Soo K, Seiichiro O, Hiromasa I, Yoshiharu U, Masataka W (2001) Chem Lett 8:760
19. Rajaram P, Viswanathan B, Aravamudan G, Srinivasan V, Sastri MVC (1973) Thermochim Acta 7:123
20. Sleight AW, Chamberland BI (1968) Inorg Chem 7:1672
21. Abrahams SC, Reddy JM (1965) J Chem Phys 43:2533
22. Young AP, Schwartz CM (1963) Science 141:348
23. Clearfield A, Moini A, Rudolf PR (1985) Inorg Chem 24:4606
24. Errandonea D, Somayazulu M, Häusermann D (2003) Phys Status Solidi (B) 235:162
25. Sleight AW (1972) Acta Cryst B 28:2899
26. Corbet F, Eyraud Ch (1961) Bull Soc Chim Fr 571
27. Pezerat HCR (1967) Seances Acad Sci Ser C 265:368
28. Strobel P, Le Page Y (1983) J Cryst Growth 61:329
29. Jang M, Weakley TJR, Doxsee KM (2001) Chem Mater 13:519
30. Sinhamahapatra PK, Bhattacharyya SK (1975) J Therm Anal 8:45
31. Holmes JD, Johnston KP, Doty RC, Korgel BA (2000) Science 287:1471
32. Yin YD, Lu Y, Gates B, Xia YN (2001) Chem Mater 13:1146
33. Trifirò F, Centola P, Pasquon I (1968) J Catal 1:86
34. Nakamoto K (1970) In: Infrared spectra of inorganic and coordination compounds, 2nd edn. Wiley-Interscience, New York, p 111